



An Extensive Study of Blazar Broad Emission Line: Changing-look Blazars and the Baldwin Effect

Hubing Xiao¹, Junhui Fan^{2,3,4}, Zhihao Ouyang⁵, Liangjun Hu⁶, Guohai Chen^{2,3,4}, Liping Fu¹, and Shaohua Zhang¹¹ Shanghai Key Lab for Astrophysics, Shanghai Normal University, Shanghai, 200234, People's Republic of China; hubing.xiao@shnu.edu.cn² Center for Astrophysics, Guangzhou University, Guangzhou 510006, People's Republic of China; fjh@gzhu.edu.cn³ Key Laboratory for Astronomical Observation and Technology of Guangzhou, Guangzhou, 510006, People's Republic of China⁴ Astronomy Science and Technology Research Laboratory of Department of Education of Guangdong Province, Guangzhou, 510006, People's Republic of China⁵ School of Physics and Materials Science, Guangzhou University Guangzhou, 510006, People's Republic of China⁶ Wuhu No.27 Middle School, Wuhu, 241001, People's Republic of China

Received 2022 May 17; revised 2022 July 27; accepted 2022 August 7; published 2022 September 9

Abstract

It is known that the blazar jet emissions are dominated by nonthermal radiation, while the accretion disk jets are normally dominated by thermal emission. In this work, our aim is to study the connection between the two types of emission by investigating the correlation between the blazar emission-line intensity property, which embodies the nature of an accretion disk, and the γ -ray flux property, which is the representative of jet emission. We compiled a sample of 656 blazars with available emission-line equivalent widths (EWs), the GeV γ -ray flux, and the spectral energy distribution (SED) information from the literature. In this work, we found 55 previous blazar candidates of uncertain types (BCUs) that are now identified as flat-spectrum radio quasars (FSRQs), and found 52 “changing-look” blazars based on their EWs, 45 of which are newly confirmed. These changing-look blazars have a larger accretion ratio ($\dot{M}/\dot{M}_{\text{Edd}}$) than BL Lacertae (BL Lac) objects. In addition, we suggest that the lower synchrotron peak blazars (LSPs) could be the source of changing-look blazars because 90.7% of the changing-look blazars in this work are confirmed as LSPs. An anticorrelation between EW and continuum intensity, the so-called global “Baldwin effect” (BEff), has been confirmed. We suggest that the steeper global BEff observed for the blazar than for radio-quiet active galactic nuclei (RQ-AGNs) is caused by the inverse Compton scattering of broad-emission-line photons. This interpretation is further supported by the positive correlation between the emission-line EW and intrinsic inverse Compton luminosity.

Key words: Blazars – Flat-spectrum radio quasars*Supporting material:* machine-readable table

1. Introduction

Blazars, one of the most extreme subclasses of active galactic nuclei (AGNs), show extreme observational properties, such as rapid and strong multiwavelength variability, high and variable polarization, strong and variable γ -ray emissions, and apparent superluminal motion at radio frequencies (Wills et al. 1992; Urry & Padovani 1995; Fan 2002; Villata et al. 2006; Fan et al. 2014; Xiao et al. 2015; Gupta et al. 2016; Lister et al. 2018; Hagen-Thorn et al. 2018; Xiao et al. 2019; Abdollahi et al. 2020; Fan et al. 2021). These observational properties are characteristic of the relativistic jet, which points toward the observer. Blazars emit radiation, which is nonthermal dominated, across the entire electromagnetic spectrum. A typical blazar broadband spectral energy distribution (SED) displays a two-bump structure. The lower-energy bump peaks in the range of infrared to X-ray and is attributed to the synchrotron radiation of relativistic electrons, while the origin of the higher-energy bump that peaks at X-ray to γ -ray wavelengths is under debate. There are two models for the higher-energy bump, the leptonic model states that the higher-energy bump is attributed to the inverse Compton (IC) scattering (Blandford & Königl 1979; Sikora et al. 1994; Sokolov & Marscher 2005; H.E.S.S. Collaboration et al. 2015; Zheng & Yang 2016; Tan et al. 2020), while the hadronic model interprets

that the higher-energy bump is attributed to the proton synchrotron radiation and secondary particle cascade (Mücke & Protheroe 2001; Dimitrakoudis et al. 2012; Zheng & Kang 2013; Diltz et al. 2015; IceCube Collaboration et al. 2018; Xue et al. 2021).

Both the optical spectrum and SED are used to make classifications for blazars. Historically, blazars are divided into two classes, namely flat-spectrum radio quasars (FSRQs) and BL Lacertae (BL Lac) objects, according to their optical spectra. The former is characterized by strong emission lines with the rest-frame equivalent width (EW) of the strongest emission line greater than 5 Å, while the latter one shows featureless optical spectrum or weak emission lines with the EW of the strongest emission line less than 5 Å (Stocke et al. 1990; Stickel et al. 1991; Stocke et al. 1991; Urry & Padovani 1995; Scarpa & Falomo 1997). The separation value of 5 Å was deduced from an examination of the line strength of a representative sample of FSRQs from the Parkes catalog (Wilkes 1986), using the same limit in the selection of the X-ray selected BL Lac objects (XBLs) from the Einstein Extended Medium Sensitivity Survey (EMSS; Stocke et al. 1990). This separation value was also applied in Stickel et al. (1991) to select BL Lac objects from 1 Jy catalog of radio sources (Kühr et al. 1981), and 34 BL Lac objects were obtained. It is clear that the separation value of 5 Å is rather arbitrarily settled. A Doppler-boosted nonthermal continuum could swamp out spectral emission lines (Blandford & Rees 1978; Xiong & Zhang 2014), and an EW greater than 5 Å may be the result of a particularly low-state of jet activity.



Original content from this work may be used under the terms of the [Creative Commons Attribution 4.0 licence](https://creativecommons.org/licenses/by/4.0/). Any further distribution of this work must maintain attribution to the author(s) and the title of the work, journal citation and DOI.

Table 1
Optical, γ -Ray, and SED Parameters of 656 4LAC Blazars

4FGL Name (1)	z (2)	$EW_{H\alpha}$ (3)	$EW_{H\beta}$ (4)	EW_{Mgii} (5)	EW_{CIV} (6)	$\log L_{BLR}$ (7)	$\log F_{IC}$ (8)	f_{γ} (9)	α_{ph} (10)	Class (11)
J0001.5+2113	0.439	344.8 ± 12.91	31.29 ± 3.91	37.2 ± 2.74		43.74	-10.48	1.36E-09	2.66	F
J0004.3+4614	1.81				246.4 ± 17.19	45.07	-11.7	2.41E-10	2.58	F
J0004.4-4737	0.88			22.54 ± 5.12		44.10	-11.24	4.36E-10	2.37	F
J0006.3-0620	0.347	117.39 ± 26.82	8.33 ± 5.75			43.60	-12.04	1.40E-10	2.13	B
J0010.6+2043	0.598		172.38 ± 18.94	112.67 ± 4.28		44.34	-11.97	1.73E-10	2.32	F

Note. Column definitions: (1) 4FGL name; (2) redshift; (3) EW of $H\alpha$ emission line in units of \AA ; (4) EW of $H\beta$ emission line in units of \AA ; (5) EW of Mg II emission line in units of \AA ; (6) EW of C IV emission line in units of \AA ; (7) luminosity of the broad-emission-line region; (8) flux of IC peak; (9) integral photon flux from 1 to 100 GeV, in units of $\text{photon} \cdot \text{cm}^{-2} \cdot \text{s}^{-1}$; (10) photon index; (11) 4LAC_DR2 Classification, “B” stands for BL Lac objects, “F” stands for FSRQs, “U” stands for BCUs. Note that features in columns (2)–(6), and (8) are obtained from Paliya et al. (2021) and the features in columns (9)–(11) are obtained from Ajello et al. (2020). (This table is available in its entirety in machine-readable form.)

The classification types, which are based on the optical spectrum of AGNs and that of blazars, were harmonious until the discovery of “changing-look” AGNs (Matt et al. 2003; Bianchi et al. 2005). The shifting between Type I AGNs and Type II AGNs, or the shifting between FSRQs and BL Lac objects has brought great challenges to the AGN unification model (Marchese et al. 2012; Isler et al. 2013; Shappee et al. 2014; Mishra et al. 2021; Peña-Herazo et al. 2021). There are explanations for the shifting; among them, the sudden change of accretion ratio resulting in the shift seems promising.

The SED features, e.g., synchrotron peak frequency (ν_s) and Compton dominance, are employed to make classifications for blazars in previous works. A parabolic function is widely used to describe the blazar SEDs in the diagram of $\log \nu F_{\nu} - \log \nu$, since it was proposed in Landau et al. (1986). Nieppola et al. (2006) fitted SEDs in the form of $\log \nu F_{\nu} - \log \nu$ with parabolic function for 308 blazars and classified BL Lac objects into low synchrotron peak BL Lac objects (LBLs; $\log \nu_s < 14.5$), intermediate synchrotron peak BL Lac objects (IBLs; $14.5 < \log \nu_s < 16.5$), and high synchrotron peak BL Lac objects (HBLs; $\log \nu_s > 16.5$) based on the synchrotron peak frequency. Similarly, Fan et al. (2016) calculated SEDs by fitting the multiwavelength data with parabolic function for a larger sample of 1392 blazars and classified blazars into low synchrotron peak sources (LSPs; $\log \nu_s \leq 14.0$), intermediate synchrotron peak sources (ISPs; $14.0 < \log \nu_s \leq 15.3$), and high synchrotron peak sources (HSPs; $\log \nu_s > 15.3$). Recently, Paliya et al. (2021) proposed that Compton dominance (CD) can be considered as one such parameter to reveal the physics of the nonthermal jets in beamed AGNs, suggesting broad-emission-line blazars being more Compton-dominated sources, and separated blazars as high CD (HCD) > 1 and low CD (LCD) < 1 .

It is no doubt that the last decade has been a golden age for blazar research in high-energy bands due to the All-Sky Survey carried out by the Large Area Telescope (Fermi-LAT; Atwood et al. 2009). The fourth catalog of AGNs detected by the Fermi-LAT (4LAC_DR2; Ajello et al. 2020) between 2008 August 4 and 2016 August 2 contains 3511 sources in 4LAC_DR2, among them 3437 blazars are included. The blazar γ -ray emission from a nonthermal mechanism dominates the entire electromagnetic radiation (Ghisellini et al. 2011, 2014; Xiong & Zhang 2014).

In this work, we investigate the optical emission-line strength and γ -ray intensity (including the IC intensity) to study the thermal emission and its connection with the

nonthermal emission in blazars. In Section 2, we define our sample, and our results will be presented in Section 3. The discussions will be given in Section 4. Section 5 presents our conclusions.

2. Sample

We collect blazar emission-line profiles from Paliya et al. (2021), in which 674 Fermi sources are included. According to 4LAC_DR2 (Ajello et al. 2020), 17 out of 674 blazars in Paliya et al. (2021) are not considered as blazars. Besides, 4FGL J0014.1+1910 is excluded because it shows a noisy spectrum and gives no EW of emission lines. At last, we have a sample of 656 Fermi blazars with emission-line EW and redshift from Paliya et al. (2021), γ -ray intensity, and SED features from 4LAC_DR2 (Ajello et al. 2020). We list our sample and the parameters in Table 1. Among the 656 sources, 55 sources are classified as blazar candidates of uncertain types (BCUs), 51 sources are classified as BL Lac objects, and 550 sources are classified as FSRQs according to the classification types in 4LAC_DR2.

3. Results

3.1. The Blazars Classification

The redshift distributes from 0.027 to 4.314 with a mean value of 1.163 ± 0.665 for the blazars in our sample. There are 47 sources with a detected $H\alpha$ emission line, the average EW of $H\alpha$ is $\langle EW_{H\alpha}(\text{\AA}) \rangle = 258.53 \pm 59.21$; 160 sources with a detected $H\beta$ emission line, $\langle EW_{H\beta}(\text{\AA}) \rangle = 121.82 \pm 13.61$; 482 sources with detected Mg II emission line, $\langle EW_{Mgii}(\text{\AA}) \rangle = 79.72 \pm 9.50$; and 193 sources with detected CIV emission line, $\langle EW_{CIV}(\text{\AA}) \rangle = 106.63 \pm 9.41$.

We are able to determine the blazar type for these 55 BCUs based on their optical spectra. All of the 55 BCUs show an EW of emission lines greater than 5\AA , thus we suggest these sources are FSRQs and list them in Table 2. Based on the classic blazar type criterion of 5\AA , we find 52 blazars that show type change, denoted as changing-look blazars, including 10 FSRQs that change their types to BL Lac objects (“F \rightarrow B”) and 42 BL Lac objects that change their types to FSRQs (“B \rightarrow F”), and list them in Table 3.

Table 2
The New Classification for BCUs in Our Sample

4FGL Name (1)	z (2)	Class (3)	New Classification (4)
J0014.3-0500	0.791	U	F
J0030.6-0212	1.804	U	F
J0036.9+1832	1.595	U	F
J0040.9+3203	0.632	U	F
J0143.5-3156	0.374	U	F
J0204.8+1513	0.407	U	F
J0223.5-0928	1.005	U	F
J0226.3-1845	1.67	U	F
J0327.5-1805	0.73	U	F
J0430.2-0356	0.628	U	F
J0516.8-0509	1.417	U	F
J0621.2-4648	1.212	U	F
J0622.9+3326	1.062	U	F
J0658.1-5840	0.421	U	F
J0725.8-0054	0.128	U	F
J0728.0+6735	0.844	U	F
J0749.3+4453	0.559	U	F
J0821.1+1007	0.954	U	F
J0904.0+2724	1.721	U	F
J0904.9-5734	0.697	U	F
J0941.7+4125	0.816	U	F
J0943.7+6137	0.791	U	F
J0949.7+5819	1.424	U	F
J1017.8+0715	1.54	U	F
J1018.9+1043	0.66	U	F
J1047.9+0055	0.252	U	F
J1054.2+3926	2.635	U	F
J1124.4+2308	0.795	U	F
J1129.2-0529	0.922	U	F
J1131.4-0504	0.263	U	F
J1139.0+4033	2.361	U	F
J1159.2-2227	0.565	U	F
J1205.8+3321	1.007	U	F
J1243.0+3950	1.22	U	F
J1248.9+4840	1.856	U	F
J1319.5-0045	0.891	U	F
J1323.0+2941	1.142	U	F
J1329.4-0530	0.576	U	F
J1412.9+5018	1.53	U	F
J1418.4+3543	0.825	U	F
J1454.0+4927	2.106	U	F
J1615.6+2130	1.627	U	F
J1627.3+4758	2.32	U	F
J1720.2+3824	0.454	U	F
J1821.6+6819	1.69	U	F
J2136.2-0642	0.941	U	F
J2140.5-6731	2.009	U	F
J2211.2-1325	0.392	U	F
J2253.3+3233	0.257	U	F
J2311.7+2604	1.748	U	F
J2313.9-4501	2.877	U	F
J2318.2+1915	2.163	U	F
J2326.2+0113	1.6	U	F
J2339.6+0242	2.661	U	F
J2352.9+3031	0.876	U	F

Note. Column definitions: (1) 4FGL name; (2) redshift; (3) 4LAC_DR2 classification, “U” denotes BCU; (4) new classification, “F” denotes FSRQ.

3.2. Correlations between EW and Continuum Luminosity

We collect the continuum luminosity (L_λ) at 5100 Å, at 3000 Å, and at 1350 Å from Paliya et al. (2021), in which these continuum luminosities were calculated via empirical relations with emission

Table 3
The Changing-look Blazars in Our Sample

4FGL Name (1)	z (2)	Change (3)	$L_{\text{BLR}}/L_{\text{Edd}}$ (4)	SED Classification (5)
J0102.8+5824	0.644	F → B	0.00034	LSP
J0337.8-1157	3.442	F → B	0.00776	LSP
J0347.0+4844	2.039	F → B	0.00035	LSP
J0521.3-1734	0.347	F → B	0.00377	LSP
J0539.6+1432	2.71	F → B	0.01659	LSP
J0539.9-2839	3.104	F → B	0.00380	LSP
J0601.1-7035	2.4	F → B	0.00071	LSP
J1816.9-4942	1.7	F → B	0.01213	LSP
J2015.5+3710	0.855	F → B	0.00734	LSP
J2121.0+1901	2.04	F → B	0.00222	LSP
J0006.3-0620	0.347	B → F	0.00097	LSP
J0127.9+4857	0.065	B → F	0.00350	LSP
J0203.7+3042	0.761	B → F	0.02678	LSP
J0209.9+7229	0.895	B → F	0.00230	LSP
J0238.6+1637	0.94	B → F	0.00240	LSP
J0334.2-4008	1.359	B → F	0.04245	LSP
J0407.5+0741	1.139	B → F	0.00097	LSP
J0428.6-3756	1.11	B → F	0.00598	LSP
J0433.6+2905	0.91	B → F	0.00228	LSP
J0438.9-4521	2.027	B → F	0.00065	LSP
J0516.7-6207	1.3	B → F	0.00021	LSP
J0538.8-4405	0.896	B → F	0.00561	LSP
J0629.3-1959	1.718	B → F	0.00172	LSP
J0654.7+4246	0.129	B → F	0.00108	LSP
J0710.9+4733	1.292	B → F	0.00194	LSP
J0814.4+2941	0.374	B → F	0.00092	HSP
J0823.3+2224	0.951	B → F	0.00575	LSP
J0831.8+0429	0.174	B → F	0.00064	LSP
J0832.4+4912	0.548	B → F	0.00260	LSP
J1001.1+2911	0.556	B → F	0.00125	LSP
J1031.1+7442	0.123	B → F	0.00515	ISP
J1058.0+4305	1.308	B → F	0.00355	LSP
J1058.4+0133	0.892	B → F	0.00177	LSP
J1058.6-8003	0.581	B → F	0.00038	LSP
J1147.0-3812	1.053	B → F	0.00168	LSP
J1250.6+0217	0.954	B → F	0.00918	LSP
J1331.2-1325	0.251	B → F	0.00212	LSP
J1402.6+1600	0.245	B → F	0.00014	ISP
J1412.1+7427	0.436	B → F	0.00091	ISP
J1503.5+4759	0.345	B → F	0.00398	LSP
J1647.5+4950	0.047	B → F	0.00148	LSP
J1751.5+0938	0.322	B → F	0.00703	LSP
J1800.6+7828	0.691	B → F	0.00186	LSP
J1806.8+6949	0.05	B → F	0.00741	LSP
J1954.6-1122	0.683	B → F	0.00347	LSP
J2134.2-0154	1.283	B → F	0.00087	LSP
J2152.5+1737	0.872	B → F	0.00046	LSP
J2202.7+4216	0.069	B → F	0.00020	LSP
J2204.3+0438	0.027	B → F	0.00020	ISP
J2216.9+2421	1.033	B → F	0.00289	LSP
J2315.6-5018	0.811	B → F	0.00143	LSP
J2357.4-0152	0.816	B → F	0.00277	LSP

Note. Column definitions: (1) 4FGL name; (2) redshift; (3) blazar type change, “B” denotes BL Lac, “F” denotes FSRQ; (4) normalized broad-line region (BLR) luminosity; (5) SED classification, “LSP” denotes low synchrotron peak sources, “ISP” denotes intermediate synchrotron peak sources, and “HSP” denotes high synchrotron peak sources.

line luminosities (Shen et al. 2011; Shaw et al. 2012):

$$\log L_{3000} = (1.016 \pm 0.003) \log L_{\text{MgII}} + (1.22 \pm 0.11), \quad (1)$$

$$\log L_{1350} = (0.863 \pm 0.009) \log L_{\text{CIV}} + (7.66 \pm 0.41), \quad (2)$$

Table 4
The Correlation between EW and Continuum Luminosity

y vs x	$(a \pm \Delta a)$	$(b \pm \Delta b)$	N	r	p
log EW (H β) vs log L_{5100}	-0.08 ± 0.06	5.23 ± 2.84	156	-0.1	0.23
log EW (MgII) vs log L_{3000}	-0.24 ± 0.03	12.74 ± 1.29	481	-0.36	1.4×10^{-16}
log EW (CIV) vs log L_{1350}	-0.25 ± 0.05	13.26 ± 2.41	191	-0.33	3.9×10^{-6}

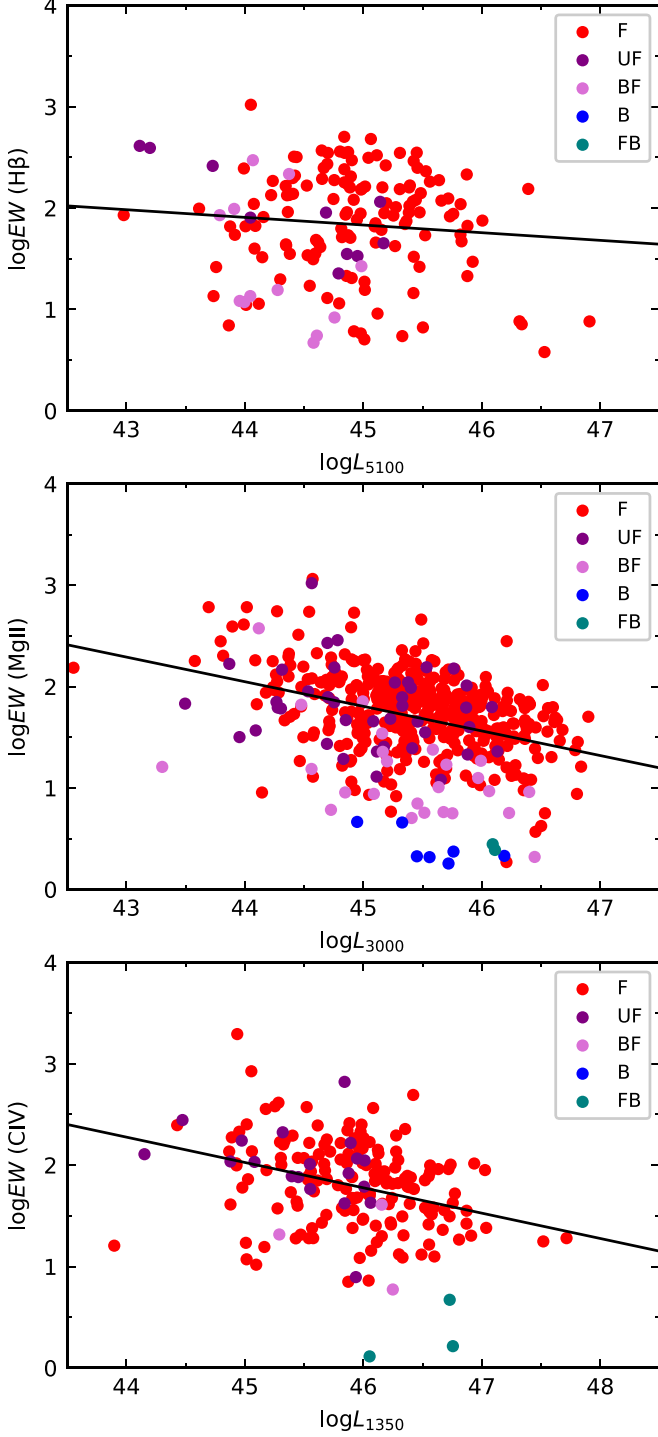


Figure 1. The correlations between emission-line (H β , Mg II, and C IV) EW and corresponding optical-continuum luminosity. “F” stands for FSRQs, “UF” stands for the new confirmed FSRQs from BCUs in this work, “BF” stands for the changing-look blazars that change from BL Lac to FSRQs, “B” stands for BL Lac objects, “FB” stands for the changing-look blazars that change from FSRQs to BL Lac objects.

$$\log L_{5100} = (0.802 \pm 0.049)\log L_{H\beta} + (1.574 \pm 0.060). \quad (3)$$

Figure 1 shows the correlations between the emission line EW and the line-continuum luminosity. The linear regression results are illustrated in Table 4, where the linear correlation is expressed as $y = (a \pm \Delta a)x + (b \pm \Delta b)$, N is the size of the considered sample, r is a correlation coefficient, and p is a chance probability.

3.3. Correlations between EW and GeV γ -Ray Parameters

Assuming that the GeV γ -ray photons follow a power-law function and is expressed as

$$\frac{dN}{dE} = N_0 E^{-\alpha_{\text{ph}}}, \quad (4)$$

where α_{ph} is the photon spectral index, and N_0 can be expressed as $N_0 = N_{(E_L \sim E_U)} \left(\frac{1}{E_L} - \frac{1}{E_U} \right)$, if $\alpha_{\text{ph}} = 2$, otherwise $N_0 = \frac{N_{(E_L \sim E_U)} (1 - \alpha_{\text{ph}})}{(E_U^{1-\alpha_{\text{ph}}} - E_L^{1-\alpha_{\text{ph}}})}$, where $N_{(E_L \sim E_U)}$ is the integral photons in units of photons $\cdot \text{cm}^{-2} \cdot \text{s}^{-1}$ in the energy range of $E_L - E_U$, and where E_L and E_U correspond to 1 GeV and 100 GeV, respectively. The integral flux, F , in units of $\text{GeV} \cdot \text{cm}^{-2} \cdot \text{s}^{-1}$, can be expressed in the form (Fan et al. 2013; Xiao et al. 2015)

$$F = N_{(E_L \sim E_U)} \frac{E_U \times E_L}{E_U - E_L} \ln \frac{E_U}{E_L} \quad (5)$$

for $\alpha_{\text{ph}} = 2$, otherwise

$$F = N_{(E_L \sim E_U)} \frac{1 - \alpha_{\text{ph}} (E_U^{2-\alpha_{\text{ph}}} - E_L^{2-\alpha_{\text{ph}}})}{2 - \alpha_{\text{ph}} (E_U^{1-\alpha_{\text{ph}}} - E_L^{1-\alpha_{\text{ph}}})}. \quad (6)$$

The γ -ray luminosity is calculated by

$$L_\gamma = 4\pi d_L^2 (1+z)^{(\alpha_{\text{ph}}-2)} F, \quad (7)$$

where $d_L = \frac{c}{H_0} \int_1^{1+z} \frac{1}{\sqrt{\Omega_m x^3 + 1 - \Omega_m}} dx$ is a luminosity distance and $(1+z)^{(\alpha_{\text{ph}}-2)}$ stands for a K -correction.

Figure 2 shows the correlations between the EW of emission lines (H α , H β , Mg II, and C IV) and the GeV γ -ray parameters (γ -ray photon spectral index α_{ph} and γ -ray luminosity L_γ). The linear regression fitting results are shown in Table 5.

4. Discussion

4.1. The Completeness of This Sample

In this work, we have compiled a sample of blazars with emission-line features from the literature. These sources are all included in 4LAC_DR2. To evaluate the completeness of our sample, we compare the redshift (z) and the γ -ray luminosity (L_γ) from our sample and from the whole Fermi blazar sample. The redshift and γ -ray luminosity distributions for blazars in our sample and for 1701 blazars with known redshift in

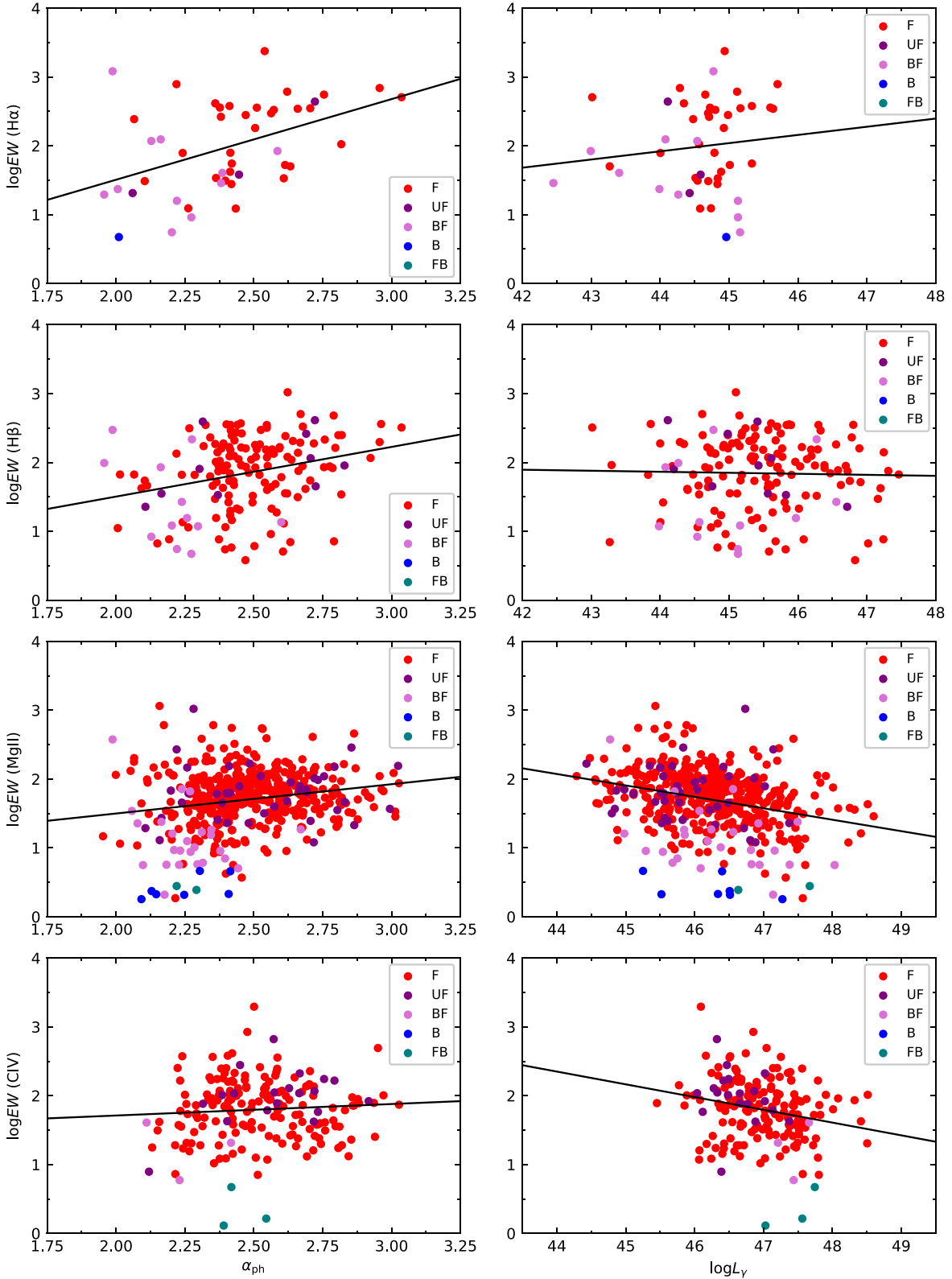


Figure 2. The correlations between emission-line (H α , H β , Mg II, and C IV) EW and GeV γ -ray parameters, photon spectral index α_{ph} (left column), and γ -ray luminosity $\log L_\gamma$ (right column). “F” stands for FSRQs, “UF” stands for the new confirmed FSRQs from BCUs in this work, “BF” stands for the changing-look blazars that change from BL Lac to FSRQs, “B” stands for BL Lac objects, and “FB” stands for the changing-look blazars that change from FSRQs to BL Lac objects.

4LAC_DR2 are shown in Figure 3. The sources in our sample (this work, hereafter TW) have larger redshift and higher γ -ray luminosity. Note that most of the 4FGL_DR2 blazars with $z < 1$ and $\log L_\gamma < 46 \text{ erg} \cdot \text{s}^{-1}$ are not included in our sample.

The redshift ranges from 0.000017 (4FGL J0654.0-4152) to 4.313 (4FGL J1510.1+5702) with an average value of $\langle z^{4LAC} \rangle = 0.80 \pm 0.66$ for the 1701 4LAC_DR2 blazars; the redshift spans from 0.027 (4FGL J2204.3+0438) to 4.314

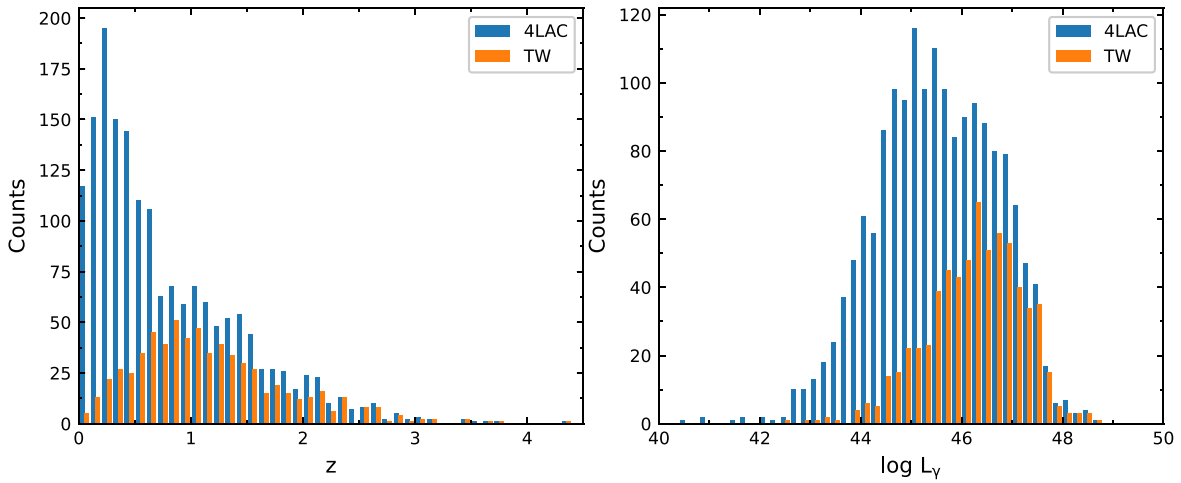


Figure 3. The redshift and γ -ray luminosity distributions of the sources in our sample and in 4LAC_DR2. The blue bar stands for 4LAC sources; the orange bar stands for the sources in our sample.

Table 5
The Correlation between EW and GeV γ -Ray Parameters

y vs x	($a \pm \Delta a$)	($b \pm \Delta b$)	N	r	p
$\log EW (H\alpha) vs \alpha_{ph}$	1.17 ± 0.35	-0.83 ± 0.85	47	0.45	0.002
$\log EW (H\alpha) vs \log L_\gamma$	0.12 ± 0.14	-3.31 ± 6.39	47	0.12	0.41
$\log EW (H\beta) vs \alpha_{ph}$	0.72 ± 0.20	0.06 ± 0.50	156	0.28	5×10^{-4}
$\log EW (H\beta) vs \log L_\gamma$	-0.01 ± 0.05	2.51 ± 2.22	156	-0.02	0.76
$\log EW (MgII) vs \alpha_{ph}$	0.43 ± 0.10	0.65 ± 0.24	481	0.20	1.6×10^{-5}
$\log EW (MgII) vs \log L_\gamma$	-0.17 ± 0.03	9.38 ± 1.17	481	-0.29	1.5×10^{-10}
$\log EW (CIV) vs \alpha_{ph}$	0.17 ± 0.17	1.38 ± 0.43	191	0.07	0.33
$\log EW (CIV) vs \log L_\gamma$	-0.19 ± 0.06	10.50 ± 2.82	191	-0.22	0.002

(4FGL J1510.1+5702) with an average value of $\langle z^{TW} \rangle = 1.16 \pm 0.66$ for the 656 blazars in our sample. The γ -ray luminosity ranges from 35.75 (4FGL J0654.0-4152) to 48.76 (4FGL J1833.6-2103) with an average value of $\langle \log L_\gamma^{4LAC} \rangle = 45.49 \pm 1.27$ for the 1701 4LAC_DR2 redshift-known blazars; the γ -ray luminosity ranges from 42.45 (4FGL J2204.3+0438) to 48.60 (4FGL J1427.9-4206) with an average value of $\langle \log L_\gamma^{TW} \rangle = 46.22 \pm 0.94$ for the 656 blazars in our sample. The Anderson–Darling (A–D) test is applied if z^{TW} and z^{4LAC} , $\log L_\gamma^{TW}$, and $\log L_\gamma^{4LAC}$ come from the same distributions. The A–D test gives statistics 123.7 and 120.8 for redshift and γ -ray luminosity, respectively. The values are both greater than the critical statistic of 6.5 for a significance level of 0.001 and this rejects the null hypothesis that two distributions come from the same distribution. Thus, we can state that our sample is not a good representative of all Fermi blazars, but a sample of brighter and more distant Fermi blazars. This sample incompleteness is caused by the selection criteria as we preferentially selected sources with emission-line features in the optical spectrum, leading us to select the brighter and more distant Fermi blazars. We caution the readers that our results are valid for this sample.

4.2. Changing-look Blazars

4.2.1. Comparing with Changing-look Blazars in Previous Works

AGNs are divided into “Type I” and “Type II” based on their optical spectra. The former displays a blue continuum from an

accretion disk and broad emission lines created by photoionization, the latter shows only narrow lines and no continuum variability (Khachikian & Weedman 1974; Peterson et al. 2004). The common understanding of these two categories is that the line of sight to the central engine is unobscured for Type I AGNs and obscured for Type II AGNs (Antonucci 1993; Urry & Padovani 1995). For the extreme AGNs, blazars are usually grouped into FSRQs and BL Lac objects based on the EW. However, these standard unification pictures for the difference between these classes meet challenges after the discovery of changing-look AGNs or blazars. The shifting between Type I AGNs and Type II AGNs was observed and reported (Matt et al. 2003; Bianchi et al. 2005; Marchese et al. 2012; Shappee et al. 2014), and the shifting was also reported between FSRQs and BL Lac objects (Isler et al. 2013, 2015; Mishra et al. 2021).

There are works exploring changing-look blazars. Peña-Herazo et al. (2021) carried out a sample of 26 changing-look blazars by searching the available optical spectra in the Large Sky Area Multi-object Fiber Spectroscopic Telescope (LAMOST) Data Release 5 (DR5) archive (Yao et al. 2019). Mishra et al. (2021) presented multiwavelength photometric and spectroscopic monitoring observations of the blazar B2 1420+32, focusing on its outbursts in 2018–2020, and suggested that this source had transitioned between BL Lac and FSRQ states multiple times.

Cross-checking the sample in Peña-Herazo et al. (2021) and Mishra et al. (2021) with our sample, it is found that seven

Table 6
The Overlapped Changing-look Blazars with Previous Works

4FGL Name (1)	Other Name (2)	P21 (3)	M21 (4)	TW (5)	Change (6)	$L_{\text{BLR}}/L_{\text{Edd}}$ (7)
J1043.2+2408	5BZQ J1043+2408	Y		N	F \rightarrow B	0.00132
J1106.0+2813	5BZQ J1106+2812	Y		N	F \rightarrow B	0.00554
J1321.1+2216	5BZQ J1321+2216	Y		N	F \rightarrow B	0.01110
J1422.3+3223	B2 1420+32		Y	N	F \rightarrow B	0.01010

Note. P21: Peña-Herazo et al. (2021); M21: Mishra et al. (2021); “Y” denotes “Yes” and “N” denotes “No.”

Table 7
The $L_{\text{BLR}}/L_{\text{Edd}}$ for Changing-look Blazars in This Work

Change type	$>5.5 \times 10^{-4}$	$<5.5 \times 10^{-4}$	$>2.8 \times 10^{-4}$	$<2.8 \times 10^{-4}$
F \rightarrow B	12	2	14	0
B \rightarrow F	36	6	38	4

sources are confirmed as changing-look blazars in common. Three of them, 4FGL J1001.1+2911 (5BZB J1001+2911), 4FGL J1402.6+1600 (5BZB J1402+1559), and 4FGL J1503.5+4759 (TXS 1501+481), are indicated as changing-look blazars in both our work and in Peña-Herazo et al. (2021). The rest of the four sources, 4FGL J1043.2+2408 (5BZQ J1043+2408), 4FGL J1106.0+2813 (5BZQ J1106+2812), 4FGL J1321.1+2216 (5BZQ J1321+2216), and 4FGL J1422.3+3223 (B2 J1420+32), that are listed in Table 6, are classified as changing-look blazars in Peña-Herazo et al. (2021) and Mishra et al. (2021), but they are not classified as changing-look blazars in the present work because of different time domains of observed spectra. 4FGL J1043.2+2408, also known as 5BZQ J1043+2408, is contained in SDSS_DR16 (Ahumada et al. 2020) with a spectrum taken in 2013 March (MJD 56,358) and was considered as an FSRQ due to a broad emission line of MgII; 4FGL J1106.0+2813, also known as 5BZQ J1106+2812, was considered as an FSRQ in this work, Paliya et al. (2021), and 4LAC_DR2 because its spectrum was taken from Shaw et al. (2012), in which this source was classified as FSRQ; 4FGL J1321.1+2216, also known as 5BZQ J1321+2216, is contained in SDSS_DR16 (Ahumada et al. 2020) with a spectrum taken in 2012 May (MJD 56,070), based on which we consider this source to be an FSRQ as also noted as an FSRQ in 4LAC_DR2. However, these three sources show clear evidence of changing-look, from FSRQs to BL Lac objects, when analyzing their latest spectra from LAMOST_DR5, in which the spectra were taken in the duration of 2015 September to 2017 June. 4FGL J1422.3+3223, known as B2 1420+32, was classified as an FSRQ by both Paliya et al. (2021) and 4LAC_DR2 based on the spectrum from SDSS_DR16, which contains the spectrum data through 2018 August. The new classification of BL Lac (Mishra et al. 2021) makes this source a changing-look blazar based on the spectroscopic study of outbursts in 2018–2020.

In total, we managed to obtain a sample of 56 changing-look blazars, in which 52 (Table 3) are found in this work and 4 (Table 6) are collected from Peña-Herazo et al. (2021) and Mishra et al. (2021). Among our 52 changing-look blazars, there are 45 newly confirmed sources.

4.2.2. The Accretion Ratio of Changing-look Blazars

The changing-look AGNs/blazars were supposed to originate from obscuration of the quasar core by dusty clouds moving in the torus, but this explanation was basically dismissed because the expected high-linear optical polarization was not widely observed (Hutsemékers et al. 2019). An alternative explanation is that the changing-look blazar arises from a sudden change in accretion rate; broad emission lines emerge when the accretion rate increases and broad emission lines disappear when the accretion rate suddenly decreases.

The blazar classification has been investigated in previous studies (Ghisellini et al. 2011; Sbarrato et al. 2012; Xiong & Zhang 2014), based on the normalized broad-line region (BLR) luminosity ($L_{\text{BLR}}/L_{\text{Edd}}$) and the normalized γ -ray luminosity ($L_{\gamma}/L_{\text{Edd}}$, in Eddington units). $L_{\text{BLR}} = \xi L_{\text{Disk}}$ and $L_{\text{Disk}} = \eta \dot{M} c^2$, where ξ is photoionization coefficient, η is energy accretion efficiency, and \dot{M} is an accretion rate; $L_{\text{Edd}} = \dot{M}_{\text{Edd}} c^2$, where \dot{M}_{Edd} is an Eddington accretion rate. Then one can get $\frac{L_{\text{BLR}}}{L_{\text{Edd}}} = \xi \eta \frac{\dot{M}}{\dot{M}_{\text{Edd}}}$ by substituting L_{BLR} and L_{Edd} . Ghisellini et al. (2011) assumed that $\dot{M}/\dot{M}_{\text{Edd}} = 0.1$, together with the assumed $\xi = \eta = 0.1$, and suggested a separation value of $L_{\text{BLR}}/L_{\text{Edd}} = 1 \times 10^{-3}$ to separate FSRQs from BL Lac objects, and FSRQs have higher $L_{\text{BLR}}/L_{\text{Edd}}$ than BL Lac objects. Later, Sbarrato et al. (2012) suggested a separation value of 5×10^{-4} by using $\dot{M}/\dot{M}_{\text{Edd}} = 0.05$. Xiao et al. (2022) suggested that $\xi = \eta = 0.1$ may not appropriate for the blazars in our sample, and proposed the use of $\xi = 0.11$ and $\eta = 0.05$. In this case, we can obtain $(L_{\text{BLR}}/L_{\text{Edd}})^{\text{TW}} = 5.5 \times 10^{-4}$ and refer to $\dot{M}/\dot{M}_{\text{Edd}} = 0.1$, or $(L_{\text{BLR}}/L_{\text{Edd}})^{\text{TW}} = 2.8 \times 10^{-4}$ and refer to $\dot{M}/\dot{M}_{\text{Edd}} = 0.05$.

We have collected $L_{\text{BLR}}/L_{\text{Edd}}$ from Xiao et al. (2022) for the 52 changing-look blazars in this work and those 4 in Peña-Herazo et al. (2021) and Mishra et al. (2021), listed them for the 56 changing-look blazars in column (4) of Table 3 and in column (7) of Table 6. We notice that 14 (taking 100%) “F \rightarrow B” and 38 (taking 90.5%) “B \rightarrow F” blazars show $L_{\text{BLR}}/L_{\text{Edd}}$ greater than 2.8×10^{-4} , which means 92.9% changing-look blazars in our sample have values of $\dot{M}/\dot{M}_{\text{Edd}}$ larger than 0.05, and that 12 (taking 85.7%) “F \rightarrow B” and 36 (taking 85.7%) “B \rightarrow F” blazars show $L_{\text{BLR}}/L_{\text{Edd}}$ greater than 5.5×10^{-4} , which means 85.7% changing-look blazars in our sample have values of $\dot{M}/\dot{M}_{\text{Edd}}$

Table 8
The Correlations between EW and the Intrinsic IC Peak Luminosity

y vs. x	($a \pm \Delta a$)	($b \pm \Delta b$)	N	r	p
$\log EW$ (H α) vs $\log L_{IC}^{in}$	0.22 ± 0.04	-7.01 ± 1.60	47	0.64	1.1×10^{-6}
$\log EW$ (H β) vs $\log L_{IC}^{in}$	0.13 ± 0.02	-3.66 ± 0.89	156	0.44	6.0×10^{-9}
$\log EW$ (MgII) vs $\log L_{IC}^{in}$	0.07 ± 0.01	-1.53 ± 0.52	481	0.27	9.1×10^{-10}
$\log EW$ (CIV) vs $\log L_{IC}^{in}$	0.08 ± 0.02	-1.58 ± 1.03	191	0.23	0.001

larger than 0.1, see Table 7. It is that the changing-look blazars mostly lie above the dividing lines proposed by Ghisellini et al. (2011) and Sbarrato et al. (2012). Pei et al. (2022) studied the correlation L_{Disk}/L_{Edd} vs L_{γ}/L_{Edd} , assuming $L_{Disk} = 10L_{BLR}$, and it was clearly shown in Figure 5 of their work that the FSRQs and the changing-look blazars have larger accretion ratios than the BL Lac objects. They have proposed an ‘‘appareling zone,’’ $2.0 \times 10^{-4} \leq L_{BLR}/L_{Edd} \leq 8.5 \times 10^{-3}$, to select changing-look blazar candidates, and we found that there are 46 (taking 82.1%) changing-look blazars in our sample that lie in this zone. Thus, the changing-look blazars have a larger accretion ratio than the normal BL Lac objects, which are believed to have a lower accretion ratio. Our result supports the explanation that the changing-look originated from the sudden change in accretion rate.

4.2.3. SED Classification of Changing-look Blazars

Blazars are also divided into LSPs, ISPs, and HSPs based on their synchrotron peak locations. We notice that among the 56 changing-look blazars, there are 54 sources with available SED classification from 4LAC_R2, and 2 ‘‘B \rightarrow F’’ sources, 4FGL J0127.9+4857 and 4FGL J0823.3+2224, without SED classification. For the 54 blazars with SED classification, all 14 ‘‘F \rightarrow B’’ blazars are associated with LSPs, 35 ‘‘B \rightarrow F’’ blazars are associated with LSPs, 4 ‘‘B \rightarrow F’’ blazars are associated with ISPs, and 1 ‘‘B \rightarrow F’’ blazar is associated with HSPs. It makes 90.7% of changing-look blazars LSPs, and thus, only a small fraction of ISPs or HSPs are associated with changing-look blazars. In this case, the LSPs could be a bank of changing-look blazars, especially for the LBLs.

4.3. The Correlations

4.3.1. The Correlation between EW and the GeV γ -Ray Parameters

Figure 2 illustrates the correlation between the EW of emission lines and the γ -ray photon index, and the observed γ -ray luminosity. We note that there are positive correlations (with p values less than 0.05), according to the fitting results in Table 5, between $\log EW$ and α_{ph} for H α , H β , and MgII. Meanwhile, a positive trend (with p values greater than 0.05) between $\log EW$ and α_{ph} for CIV is found. The positive correlation and trend suggest that the stronger the emission line the softer the GeV spectrum. There are anticorrelations between $\log EW$ and $\log L_{\gamma}$ for MgII and CIV, but this anticorrelation is not found for either H α or H β .

4.3.2. The Baldwin Effect

The correlation between the EW and continuum luminosity is illustrated in Figure 1 and the corresponding regression results are tabulated in Table 4. A trend of anticorrelation between $\log EW$ (H β) and $\log L_{5100}$ shows up and solid anticorrelations between $\log EW$ (MgII) and $\log L_{3000}$, and

between $\log EW$ (CIV) and $\log L_{1350}$ are found. Our results of the anticorrelations are consistent with the results reported in many other previous works (Dietrich et al. 2002; Shields 2007; Kovačević et al. 2010; Shemmer & Lieber 2015; Patiño-Álvarez et al. 2016; Rakić et al. 2017).

The anticorrelation between the broad-line EW and the continuum luminosity of single-epoch observations of a large number of AGNs are known as the global ‘‘Baldwin effect’’ (hereafter BEff; Baldwin 1977; Carswell & Smith 1978). The BEff indicates that the line flux is increasing more slowly than the local continuum (or is constant) because EW is the ratio of line flux to the local continuum flux. The BEff is well established for broad emission lines in the UV/optical regions (Dietrich et al. 2002; Shields 2007), even for narrow lines (e.g., Dietrich et al. 2002; Kovačević et al. 2010), and it is found that it steepens with increasing ionization potential (Zheng & Malkan 1993). Various mechanisms have been proposed as possible interpretations of the BEff, such as a luminosity-dependent ionization continuum and the BLR covering factor (Mushotzky & Ferland 1984; Zheng & Malkan 1993), the geometrical effect of an inclination-dependent anisotropic continuum (Netzer 1985), different variability patterns in the thermal and nonthermal components of the continuum (Kinney et al. 1990; Patiño-Álvarez et al. 2016), or processes that involve a different Eddington ratio or black hole mass (Xu et al. 2008; Bian et al. 2012), etc. The most widely accepted explanation is that the ionization continuum softens as the luminosity increases (Zheng & Malkan 1993), so that high-luminosity AGNs decrease the fraction of ionizing photons for broad-emission-line formation.

In this work, we found a slope of -0.08 ± 0.06 for the correlation between EW of H β emission line and continuum luminosity at 5100 Å; however, a chance probability of 0.23 suggests the correlation is not evident. Rakić et al. (2017) obtained a slope of -0.0467 of $EW(H\beta)$ against L_{5100} in a logarithmic diagram, and claimed that no evidence of significant BEff for H β emerged. Both of the results, in this work and in Rakić et al. (2017), agree with previous findings, which concluded that no BEff was present in the broad Balmer lines (Dietrich et al. 2002; Kovačević et al. 2010). But, the BEff is found for MgII and CIV emission lines with slopes of -0.24 ± 0.03 and of -0.25 ± 0.05 (see Table 4) in this work. Our results are consistent with the results of BEff for MgII and CIV emission lines in Patiño-Álvarez et al. (2016), in which they found the BEff for these two lines and reported that slopes of 0.20 and 0.21 were derived, respectively.

It is found that there is a difference in BEff anticorrelation between blazars and radio-quiet (RQ) AGNs, the former show a steeper anticorrelation than the latter one (Patiño-Álvarez et al. 2016). We suggest the steepening of BEff for blazars results from the IC scattering of broad-emission-line photons from BLR for two reasons. On one hand, consider the case that the continuum luminosity is identical for blazars and RQs; the EW for blazars should be smaller than it is for RQs because a significant number of broad-emission-line photons are fed to

the IC process, and scattered to the γ -ray band, resulting in a high Compton dominance (Abdo et al. 2010; Ghisellini et al. 2011; Paliya et al. 2021) and a weaker emission line. On the other hand, when the continuum luminosity gets stronger, the bolometric luminosity should increase. The bolometric luminosity is dominated by the IC emission (or the γ -ray luminosity; Ghisellini & Tavecchio 2010; Ghisellini et al. 2014; Xiong & Zhang 2014; Xiao et al. 2022); therefore, increased bolometric luminosity yields more external photons (e.g., broad-emission-line photons) to feed the IC process. Then the emission lines of blazars (mainly FSRQs) get weaker and the difference on EW become larger with the increase of continuum luminosity compared to the RQs. Consequently, a steepening of BEff is formed for blazars.

In this scenario, it is natural that strong emission lines should be able to contribute more seed photons to the IC process; therefore, we can expect a positive correlation between EW and IC luminosity.

We collected the flux of the IC peak (F_{IC}) from Paliya et al. (2021) to calculate the IC peak luminosity ($L_{IC} = 4\pi d_L^2 F_{IC}$, in the observer frame). However, the observed IC luminosity is boosted by a Doppler beaming effect (Dermer 1995; Paliya et al. 2015, 2021) and gives the intrinsic IC luminosity (in the source rest frame) as $L_{IC}^{in} = L_{IC}/\delta^4$, where δ is the Doppler factor. Doppler factors are available in different literature and are given in discrepancy. In this work, we employ the method that was proposed by Zhang et al. (2020), in which they proposed to use γ -ray luminosity and broad-line-region luminosity (L_{BLR}) to calculate δ of γ -ray emission and to calculate δ for our sources. The data of L_{BLR} are calculated based on the work of Paliya et al. (2021) and Xiao et al. (2022).

The results between EW and intrinsic IC luminosity are shown in Table 8 and in Figure 4. The results illustrate that the EW is positively correlated with intrinsic IC luminosity, suggesting that sources with the stronger intrinsic IC luminosity tend to have stronger emission lines. Moreover, these results have confirmed our prediction, there is a positive correlation between EW and inverse Compton luminosity, and have proven that the steepening of BEff for blazars (mostly FSRQs) is, indeed, caused by the IC scattering of broad-emission-line photons.

5. Conclusion

In this work, we aim to study the emission-line property and its connection with the nonthermal emission of blazars. We collected the EW of emission lines, γ -ray emission, and SED information for a sample of 656 Fermi blazars. We have studied the blazar classification according to the EW and the correlation between the EW and γ -ray luminosity, and the global BEff.

Our main results are as follows: (1) There are, out of the 656 Fermi blazars, 55 previously classified as BCUs are now classified as FSRQs. (2) We find 52 changing-look blazars through the study of the EW, among them there are 10 FSRQs that change to BL Lac objects and 42 BL Lac objects that change to FSRQs. Besides this, 45 of them are newly confirmed as changing-look blazars. (3) The accretion rates (\dot{M}/\dot{M}_{Edd}) of the 52 changing-look blazars are calculated. We notice that there are 92.9% changing-look blazars in our sample

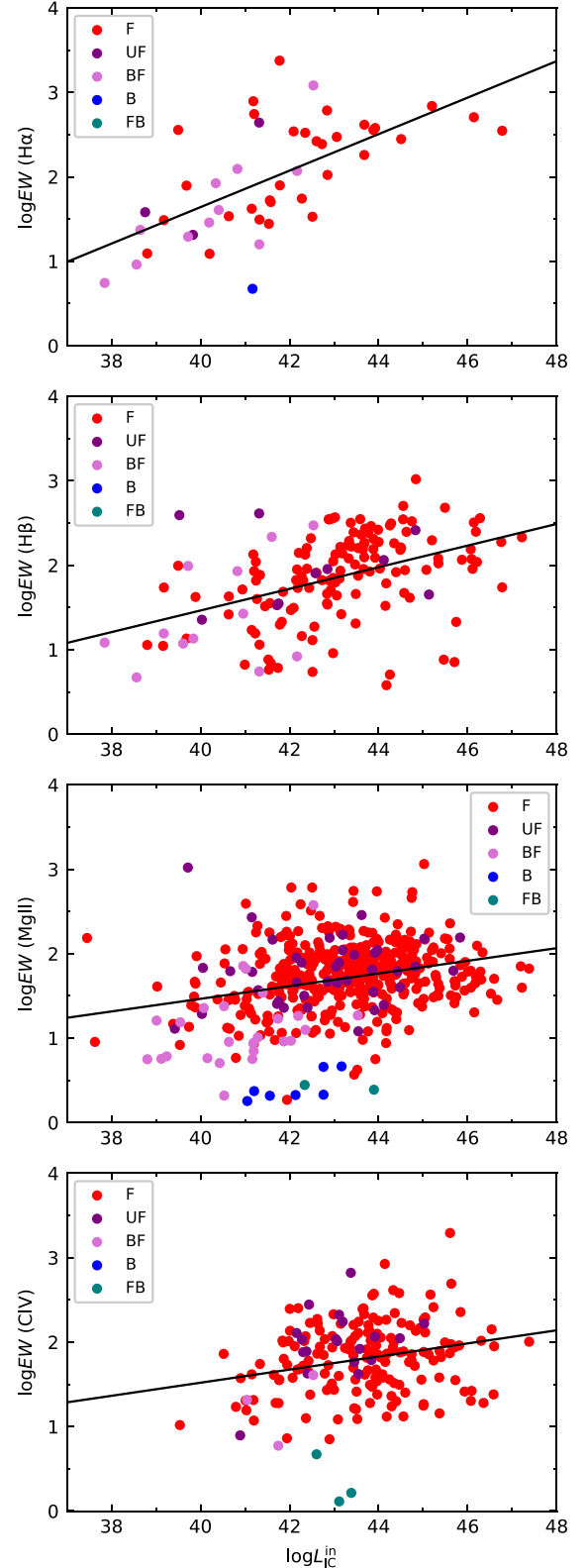


Figure 4. The correlations between emission line ($H\alpha$, $H\beta$, $Mg II$, and $C IV$) EW and the intrinsic IC luminosity ($\log L_{IC}^{in}$). “F” stands for FSRQs, “UF” stands for the new confirmed FSRQs from BCUs in this work, “BF” stands for the changing-look blazars that change from BL Lac to FSRQs, “B” stands for BL Lac objects, “FB” stands for the changing-look blazars that change from FSRQs to BL Lac objects.

with $\dot{M}/\dot{M}_{\text{Edd}} > 0.05$ and 85.7% changing-look blazars in our sample with $\dot{M}/\dot{M}_{\text{Edd}} > 0.1$, suggesting that the changing-look blazars have a larger accretion ratio. Besides this, we notice that 90.7% of the changing-look blazars in this work are LSPs and suggest that the LSPs are a bank of changing-look blazars. (4) The global BEff is confirmed for blazars (mostly FSRQs) in this work and the results indicate a steeper anticorrelation of EW (log EW) against continuum luminosity (log L_{3000} and log L_{1350}) than that of the RQ AGNs. (5) We propose that the steepening of global BEff is caused by the IC scattering of broad-emission-line photons and predict a positive correlation between the EW (log EW) and the IC luminosity (log L_{IC}). This prediction is indeed correct and the EW of H α , H β , Mg II, and CIV are positively correlated with the intrinsic IC peak luminosity.

We thank the support from our laboratory, the key laboratory for astrophysics of Shanghai, and we thank Dr. Vaidehi S. Paliya for his kindly help and for sharing data. Meanwhile, L.F. acknowledges the support from the National Natural Science Foundation of China (NSFC) grants 11933002, STCSM grants 18590780100, 19590780100, SMEC Innovation Program 2019-01-07-00-E00032, and Shuguang Program 19SG41. S.Z. acknowledges the support from the Natural Science Foundation of Shanghai (20ZR1473600). J.F. acknowledges the support by the NSFC (NSFC U2031201 and NSFC 11733001).

ORCID iDs

Hubing Xiao  <https://orcid.org/0000-0001-8244-1229>
Junhui Fan  <https://orcid.org/0000-0002-5929-0968>
Shaohua Zhang  <https://orcid.org/0000-0001-8485-2814>

References

- Abdo, A. A., Ackermann, M., Agudo, I., et al. 2010, *ApJ*, 716, 30
 Abdollahi, S., Acero, F., Ackermann, M., et al. 2020, *ApJS*, 247, 33
 Ahumada, R., Prieto, C. A., Almeida, A., et al. 2020, *ApJS*, 249, 3
 Ajello, M., Angioni, R., Axelsson, M., et al. 2020, *ApJ*, 892, 105
 Antonucci, R. 1993, *ARA&A*, 31, 473
 Atwood, W. B., Abdo, A. A., Ackermann, M., et al. 2009, *ApJ*, 697, 1071
 Baldwin, J. A. 1977, *ApJ*, 214, 679
 Bian, W.-H., Fang, L.-L., Huang, K.-L., & Wang, J.-M. 2012, *MNRAS*, 427, 2881
 Bianchi, S., Guainazzi, M., Matt, G., et al. 2005, *A&A*, 442, 185
 Blandford, R. D., & Königl, A. 1979, *ApJ*, 232, 34
 Blandford, R. D., & Rees, M. J. 1978, in Pittsburgh Conf. on BL Lac Objects (Pittsburgh, PA: Univ. of Pittsburgh), 328
 Carswell, R. F., & Smith, M. G. 1978, *MNRAS*, 185, 381
 Dermer, C. D. 1995, *ApJL*, 446, L63
 Dietrich, M., Hamann, F., Shields, J. C., et al. 2002, *ApJ*, 581, 912
 Diltz, C., Böttcher, M., & Fossati, G. 2015, *ApJ*, 802, 133
 Dimitrakoudis, S., Mastichiadis, A., Protheroe, R. J., & Reimer, A. 2012, *A&A*, 546, A120
 Fan, J.-H. 2002, *PASJ*, 54, L55
 Fan, J.-H., Bastieri, D., Yang, J.-H., et al. 2014, *RAA*, 14, 1135
 Fan, J.-H., Yang, J.-H., Liu, Y., & Zhang, J.-Y. 2013, *RAA*, 13, 259
 Fan, J. H., Yang, J. H., Liu, Y., et al. 2016, *ApJS*, 226, 20
 Fan, J. H., Kurtanidze, S. O., Liu, Y., et al. 2021, *ApJS*, 253, 10
 Ghisellini, G., & Tavecchio, F. 2010, *MNRAS*, 409, L79
 Ghisellini, G., Tavecchio, F., Foschini, L., & Ghirlanda, G. 2011, *MNRAS*, 414, 2674
 Ghisellini, G., Tavecchio, F., Maraschi, L., Celotti, A., & Sbaratto, T. 2014, *Natur*, 515, 376
 Gupta, A. C., Agarwal, A., Bhagwan, J., et al. 2016, *MNRAS*, 458, 1127
 H.E.S.S. Collaboration, Abramowski, A., Aharonian, F., et al. 2015, *A&A*, 573, A31
 Hagen-Thorn, V. A., Larionov, V. M., Morozova, D. A., et al. 2018, *ARep*, 62, 103
 Hutsemékers, D., Agís González, B., Marin, F., et al. 2019, *A&A*, 625, A54
 IceCube Collaboration, Aartsen, M. G., Ackermann, M., et al. 2018, *Sci*, 361, eaat1378
 Isler, J. C., Urry, C. M., Coppi, P., et al. 2013, *ApJ*, 779, 100
 Isler, J. C., Urry, C. M., Bailyn, C., et al. 2015, *ApJ*, 804, 7
 Khachikian, E. Y., & Weedman, D. W. 1974, *ApJ*, 192, 581
 Kinney, A. L., Rivolo, A. R., & Koratkar, A. P. 1990, *ApJ*, 357, 338
 Kovačević, J., Popović, L. Č., & Dimitrijević, M. S. 2010, *ApJS*, 189, 15
 Kühn, H., Witzel, A., Pauliny-Toth, I. I. K., & Nauber, U. 1981, *A&AS*, 45, 367
 Landau, R., Golisch, B., Jones, T. J., et al. 1986, *ApJ*, 308, 78
 Lister, M. L., Aller, M. F., Aller, H. D., et al. 2018, *ApJS*, 234, 12
 Marchese, E., Braitto, V., Della Ceca, R., Caccianiga, A., & Severgnini, P. 2012, *MNRAS*, 421, 1803
 Matt, G., Guainazzi, M., & Maiolino, R. 2003, *MNRAS*, 342, 422
 Mishra, H. D., Dai, X., Chen, P., et al. 2021, *ApJ*, 913, 146
 Mücke, A., & Protheroe, R. J. 2001, *Aph*, 15, 121
 Mushotzky, R., & Ferland, G. J. 1984, *ApJ*, 278, 558
 Netzer, H. 1985, *MNRAS*, 216, 63
 Nieppola, E., Tornikoski, M., & Valtaoja, E. 2006, *A&A*, 445, 441
 Paliya, V. S., Domínguez, A., Ajello, M., Olmo-García, A., & Hartmann, D. 2021, *ApJS*, 253, 46
 Paliya, V. S., Sahayanathan, S., & Stalin, C. S. 2015, *ApJ*, 803, 15
 Patiño-Álvarez, V., Torrealba, J., Chavushyan, V., et al. 2016, *FRASS*, 3, 19
 Peña-Herazo, H. A., Massaro, F., Gu, M., et al. 2021, *AJ*, 161, 196
 Pei, Z., Fan, J., Yang, J., Huang, D., & Li, Z. 2022, *ApJ*, 925, 97
 Peterson, B. M., Ferrarese, L., Gilbert, K. M., et al. 2004, *ApJ*, 613, 682
 Rakić, N., La Mura, G., Ilić, D., et al. 2017, *A&A*, 603, A49
 Sbaratto, T., Ghisellini, G., Maraschi, L., & Colpi, M. 2012, *MNRAS*, 421, 1764
 Scarpa, R., & Falomo, R. 1997, *A&A*, 325, 109
 Shappee, B. J., Prieto, J. L., Grupe, D., et al. 2014, *ApJ*, 788, 48
 Shaw, M. S., Romani, R. W., Cotter, G., et al. 2012, *ApJ*, 748, 49
 Shemmer, O., & Lieber, S. 2015, *ApJ*, 805, 124
 Shen, Y., Richards, G. T., Strauss, M. A., et al. 2011, *ApJS*, 194, 45
 Shields, J. C. 2007, in ASP Conf. Ser. 373, The Central Engine of Active Galactic Nuclei, ed. L. C. Ho & J. W. Wang (San Francisco, CA: ASP), 355
 Sikora, M., Begelman, M. C., & Rees, M. J. 1994, *ApJ*, 421, 153
 Sokolov, A., & Marscher, A. P. 2005, *ApJ*, 629, 52
 Stöckel, M., Padovani, P., Urry, C. M., Fried, J. W., & Kuehr, H. 1991, *ApJ*, 374, 431
 Stocke, J. T., Morris, S. L., Gioia, I., et al. 1990, *ApJ*, 348, 141
 Stocke, J. T., Morris, S. L., Gioia, I. M., et al. 1991, *ApJS*, 76, 813
 Tan, C., Xue, R., Du, L.-M., et al. 2020, *ApJS*, 248, 27
 Urry, C. M., & Padovani, P. 1995, *PASP*, 107, 803
 Villata, M., Raiteri, C. M., Balonek, T. J., et al. 2006, *A&A*, 453, 817
 Wilkes, B. J. 1986, *MNRAS*, 218, 331
 Wills, B. J., Wills, D., Breger, M., Antonucci, R. R. J., & Barvainis, R. 1992, *ApJ*, 398, 454
 Xiao, H., Ouyang, Z., Zhang, L., et al. 2022, *ApJ*, 925, 40
 Xiao, H., Fan, J., Yang, J., et al. 2019, *SCPMA*, 62, 129811
 Xiao, H. B., Pei, Z. Y., Xie, H. J., et al. 2015, *Ap&SS*, 359, 39
 Xiong, D. R., & Zhang, X. 2014, *MNRAS*, 441, 3375
 Xu, Y., Bian, W.-H., Yuan, Q.-R., & Huang, K.-L. 2008, *MNRAS*, 389, 1703
 Xue, R., Liu, R.-Y., Wang, Z.-R., Ding, N., & Wang, X.-Y. 2021, *ApJ*, 906, 51
 Yao, S., Wu, X.-B., Ai, Y. L., et al. 2019, *ApJS*, 240, 6
 Zhang, L., Chen, S., Xiao, H., Cai, J., & Fan, J. 2020, *ApJ*, 897, 10
 Zheng, W., & Malkan, M. A. 1993, *ApJ*, 415, 517
 Zheng, Y. G., & Kang, T. 2013, *ApJ*, 764, 113
 Zheng, Y. G., & Yang, C. Y. 2016, *MNRAS*, 457, 3535